Deep Learning for Radiation Dose Estimation

Masterarbeit

Eingereicht von:	Gutwein, Simon
Studiengang:	Medizinische Strahlenwissenschaften
Matrikelnummer:	5419474
Betreuer:	Prof. Dr. Daniela Thorwarth
Bearbeitungszeit:	von 16.09.2021
	bis 16.03.2022

Eberhard Karls Universität Tübingen

Universitätsklinik für Radioonkologie // Sektion für Medizinische Physik

Hoppe-Seyler-Straße 6, 72076 Tübingen

Abstract

Hello, here is some text without a meaning. This text should show what a printed text will look like at this place. If you read this text, you will get no information. Really? Is there no information? Is there a difference between this text and some nonsense like “Huardest gefburn”? Kjift – not at all! A blind text like this gives you information about the selected font, how the letters are written and an impression of the look. This text should contain all letters of the alphabet and it should be written in of the original language. There is no need for special content, but the length of words should match the language.

Contents

List of Figures

List of Tables

Abkürzungsverzeichnis

1 Introduction

Introduction

- **Genereller Ablauf am MR-Linac stand jetzt**
- Person kommt, bekommt ein CT für initiale Planung, danach wird dann bei Bestrahlung des Patienten ein MRT von dem Patienten gemacht. Registrierung von CT und MRT und adaption von contours auf MRT. Dann Online-Plan adaption bei dem Plan aufgrund von adapt to position oder shape. Results in no adaption or adaption of segments shape, monitor units or both. This is repeated for each treatment fraction of the patient (Adaptive radiotherapy: The Elekta Unity MR-linac concept)
- **Wie soll der Ablauf einmal aussehen beim MR-Linac**
- Goal is to achieve a MRi-only treatment workflow, including imaging with MRI contouring on MRI and planning and calculation of plans on mri. dose calculation is not possible on mri data because mri is not a quantitative imaging modality, meaning pixel values give no information about the electron density of the underlying tissue or body part. therefore synthetic ct images need to be created from mri images, which enable dose calculations.
- **Und dann auf Dosisdeposition eingehen / Was ist aktuelle Methode** hier noch viel verschieben nach material und methodik
- (http://dx.doi.org/10.1118/1.2795842) monte carlo simulations are currently used for dose calculation for radiotreatment plans in a clinical setting. The interactions of photons in human tissue in the energy spectrum of interest for external beam therapy transfer the photon energy on to electrons or positrons. these particles then transfer their energy into the surrounding tissue. before energy deposition the photon and especially the electron undergo a number of elastic and non elsatic interactions with atoms. In the process the main energy loss is caused by inelastic collisions and radiative interactions. the collisions result in ionization and therefore secondary electrons. radative interactions result in a energy trasnfer back to photons. the sum of these phenomena in a photon field results in a coupled electron-photon shower, which can be described by a coupled set of integrodifferntial transport equations. due to the lack of a analystical solution, without any major simplifications and assumptions for conditions, the monte carlo algorithm is

used to simululate a multitude of particle histories in the desired target volume. partical histories describe the exact way of a photon from the source to its point in the volume were it has lost all of its energy including enery transport to secondary electrons in the process of collisions. the stochastic nature of the interaction processes of photons and electrons need for a large number of simulated particles to achieve an accurate result of dose deposition. the entirety of all simulated particles then results in an accurate dose distribution which can be used for treatment planning. the need for particle histories in the magnitude of 10^7 to 10^{11} for accurate dose estimations, result in long simulation times.

- Wo findest Deep Learning Anwendung (Bezug zu Medizin)
- Deep learning and especially computer vision is already present in current research of Biology, Physics as well as medicine. there are a multiple fields in which CV can be applied to fields such as dermatology (https://sci-hub.ru /10.1038/nature21056), radiology (https://sci-hub.ru /10.1038/srep24454, https://sci-hub.ru /10.1097/rli.0000000000000
cardiology (https://arxiv.org/abs/1708.09843) or pathology (https://www.nature.com/articles/
020-58467-9.pdf)
- Einleitung zu Deep Learning
- . deep learning is a prefered tool due to its short inference times aswell as super human performance level on certain tasks. the implementation of the fully convulitional network (https://arxiv.org/pdf/1411.4038.pdf) and its further development of the U-Net utilizing data from higher level representations of the data in the form of skip connections (https://arxiv.org/abs/1505.04597) have revolutionized the application of deep learning for image data and 3d data i the form of a 3D-UNets.
- Was ist die Contribution / Aims <- Ziel: Dosisvorhersage mit DL, möglichst robust
- In this paper we investiage the capabilities of deep learning in the field of dose predictions for radio treatment plans. we aimed to achieve a robust dose prediction irrespective of the body region of interest and irresprective of the complexity of the treatment plan.
-

Show why Radiotherapy is so important: search for sources of application of radiotherapy for different entities. Prostate: [1–3] Mamma: [4–6] Head & Neck: [7–10] Liver: [11–15] Lymph Nodes: [16–20]

Was ich noch brauche: Infos über MR-Linac, was ist die Vision hinter dem MR Linac (online adaption)

The use of Magnet Resonace Imaging (MRI) during radiotherapy has opened a variety of new opportunities for treatment optimization. MRI provides a better contrast in soft tissue areas of the body, compared to conventional computed tomograpy (CT), and can be used to assess functional image data from the patient in real time. The enhanched contrast leads to better organs at risk (OAR) and tumor volume delineation. (doi:10.1016/S0360-3016(03)01446-9). Recent research efforts are exploring the capabilities of the hybrid MRI linear accelerator (MRI-Linac) (doi:10.1007/s00066-018-1386-z, doi:10.1016/j.radonc.2007.10.034, doi:10.1002/acm2.12233). The introduction of the MRI-Linac has transformed the clinical workflow for radiotherapy as well as treatment planning. Patients are required to receive one CT for initial treatment planning. For radiation in each fraction, the inital plan is registrated on the current MRI and optionally adapted to shift or size variation of the tumor volume (doi:10.1016/j.ctro.2019.04.001). Goal is to reach an MRI-only-workflow where image acquisition, treatment planning and radiotherapy only involve the MRI-Linac. To achieve this goal multiple steps in the clinical workflow need to be adapted

behind MRI Linac is an radiotreatment adaption in an onine manner, meaning that a shift of the tumor volume and changes to the patients anatomy due to movement can be considered to adapt the treatmentplan. This results in smaller safety margins (doi:10.1102/1470-7330.2004.0054) for tumor volumes and ultimately result in a lower delivered dose to organs at risk. To achieve this ultimate goal, multiple steps, such as anatomy segmentation, treatmentplan adaption and dose deposition simulations need to be able to be performed in real-time.

Welche besonderheiten gibt es bei einem MR-Linac im Vergleich zu einem normalem Bestrahler (Stichworte: ERE, Electron Deposition Shift) Wie funktioniert normale Dosisberechung (Monte Carlo doi:10.1118/1.598917), warum ist der Nutzen davon limitiert wenn man in die online Adaption möchte.

However, since MC simulation is a stochastic process, the resulting dose map contains inherent quantum noise whose variance is inversely proportional to the number of the simulation histories and, accordingly, to the simulation time. Typically, achieving clinically acceptable precision requires hours of CPU computation time. Graphics processing unit (GPU)-based parallel computation frameworks can accelerate MC simulation to a few minutes for a typical IMRT/VMAT plan (doi:10.1088/0031-9155/55/11/006)

However, several areas in the clinical workflow require real-time dose calculation, such as

inverse optimization of the treatment planning process for IMRT and VMAT (doi:10.1088/2632-2153/abdbfe) especially online radiotherapy and online plan adaption are limited by the time needed to recalculate dose distributions of beam settings and patient anatomies due to moving organs (doi:10.1016/j.clon.2018.08.001)

Machine Learning Teil: Wie wird Machine Learning in verschiedenen bereichen der bestrahlungsplanung bezüglich MRI genutzt: Eine Implementierung und Nutzung dieser könnte zum Erreichen einer Online-Bestrahlnugsadaption führen

1. Autosegmentation ([21, 22]) aswell as uncertrainty ([23])
2. Radio Treatment Plan optimization ([24, 25])
3. Dose Estimation ([26, 27] active denoising of lower history MC Simulations (doi:10.1002/mp.13856))
4. Pseudo CT ([28–30])

2 Previous Work

Previous Work (evtl. mit in die Introduction) / Related Work

- Bezug nehmen auf
- DeepDose
- Weitere Paper zu dem Thema (Protonen mit LSTM, weitere Dosisberechnungen, siehe Paper, dass Christian gesendet hat)

Radiotherapy:

https://iopscience.iop.org/article/10.1088/1361-6560/ab7630
using 3d unet architecture and patch based approach to estimate dose in prostate cancer patients for individual segments of an entire treatmentplan. input data fro unet include patient information in the form of ct, as well as information form the accellerator such as beam angle and beam shape. they achieve very good results with 99.9 ± 0.3 for 3%/3mm gamma passrate. and 1 minute for dose estimation for one patient in total

https://aapm.onlinelibrary.wiley.com/doi/full/10.1002/mp.14658
dose prediction for protonfields in highly heterogenous tissues using long short term memory (LSTM) networks. it treats the affected part of the tissue as a sequence of 2 inputs and calculates the respective dose in the scheme of a marching beam trough the tissue. the reach robustnes by generating artificial phantom cases for the dose predictions. results show 98.57% gamma passrate (1%/3mm) for artificial cases and an average gama passrate of 97.85% for patient test cases.

https://www.ncbi.nlm.nih.gov/pmc/articles/PMC7870566/
dose estimation for segments was achieved by combining fluence maps from segments aswell as patient anatomies. they generated 3d fluence volumes from 2d fluence maps including information of beam angle. an 3d unet like architecture with residual blocks inside the convolutional building block was used for prediction. the overall dose variation normalized to the prescribed dose was 0.17% ± 2.28%.

High-Particle Simulation of Monte-Carlo Dose Distribution with 3D ConvLSTMs
to achieve a precise dose distribution in the desired 3d volume they use an approach utilizing active denoising of monte carlo simulations with deep learning. they implemented a 3d LSTM architecture inside the skipconnection of a 3d unet architecture. a sequence of noisy monte carlo simulations was used as the input and the output is the denoised

doe prediction. the loss function was constructed from the L1 loss and the structural similarity index measure. gamma pass rate for 5 patients was 94.1% ± 1.2% and the L1 was was $4{\cdot}10^{-3} \pm 1{\cdot}10^{-3}$.

DeepMCDose: A Deep Learning Method for Efficient Monte Carlo Beamlet Dose Calculation by Predictive Denoising in MR-Guided Radiotherapy the proposed network consists of 3 seperate Unets to seperately analyse the 3 input channels consisting of unsersampled MC dose, MC x-ray fluence and the ct geometry for a single beamlet. the output from each network is then combined to calculate the residual needed dose to achieve the denoised dose distribution. the normalized mean absolute error reduced from 25.7% on the undersamplet MC simulation to 0.106% for the network output. The simulation of 380s for an fully sampled beamlet was reduced to 220 ms for the network prediction

https://www.ncbi.nlm.nih.gov/pmc/articles/PMC7115345/

3 Medical Knowledge

Medical Base Knowledge:

wieso schreibe ich hier über radiotherapy - wie wird sie angewendet - was ist konverntionell - linear beschleinuger, ablauf für patienten - planung dosis nebenwirkungen eingehen - auf was zielt der MR linac ab überleitung zu dosisberechnungs algorithmen - monte carlo - in detail EGSnrc eingehen und erläutern was der vorteil hier für uns ist (einzelne segmente, erläuterung, dass ein plan aus verschiedenen segmenten besteht die aufsummiert werden) kurz über wechselwirkungen reden und wie die dosisdeposition mit monte carlo simuliert wird. dann kurz erläutern warum ich das hier eigentlich grade beschreibe - darauf eingehen dass trainingsdaten halt mit diesem egsnrc simuliert werden

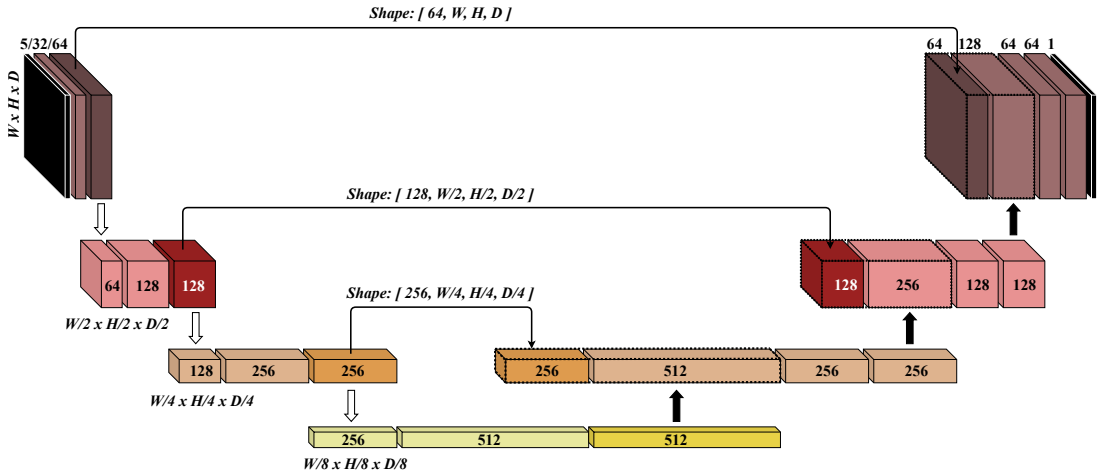

Figure 1: Network architeture scheme. Size of the input masks are depicted by width (W), height (H) and depth (D). Input dimensionality is WxHxDx5 and output dimensionality is WxHxDx1.

4 Material and Methods

Material and Methods (Unsicher wie ich das aufbauen soll)

Netzwerk Architektur Dataloading Was ist Input Wie werden Trainingsdaten erzeugt Auswertungsmetriken

- Hypothesen und wie wir diese Überprüfen: - ...

Data: Beschreibung der Patientendaten (wie viele, wie verteilt) Infos zu der Ethical... Falls in der Discussion die Feldgröße von Relevanz ist dann Infos mit rein nehmen. Nähere Infos in Tabelle

4.1 Network Architecture

3D UNet architecture with a downsampling ratio of 8 and a maximum layer depth of 512 in the bottleneck connection and skip connections before each pooling layer. multiple input masks in the size of CT with a resolution od 1.1718 x 1.1718 x 3 mm^3 resolution in coronal, sagital, and tanversal dimension respectively. shown in image fig. 1

4.2 Dataloading

Patch based training, warum erklären, dass aufgrund der Natur von 3D-Daten und dem Limit des Grafikkarten speichers nur ein teil der daten geladen werden können. erklären, dass der speicherpaltz verbrauch zum vorherigen abspeichern aller patches zu groß ist

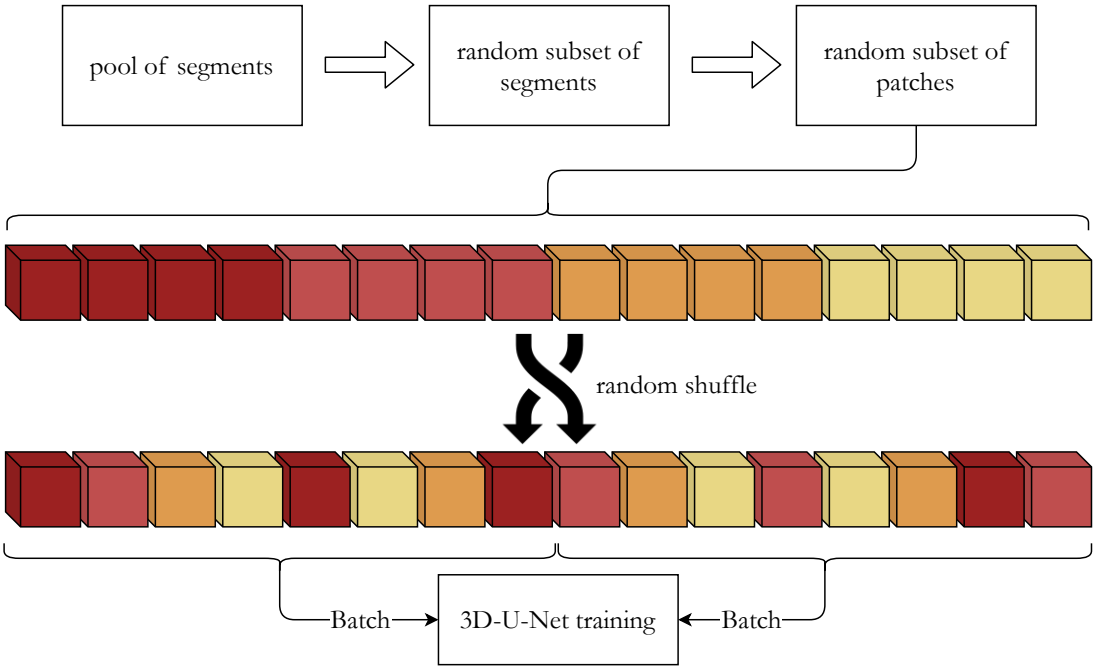

Figure 2: Memory efficient queue based dataloading for 3D patch based training. data from different segments are depicted in differnt color shades.

und die patches somit on the fly extrahiert werden mussen. eingehen auf TorchIO und deren lösung mittels einer queue an der sich meine lösung orientiert. on the fly loading von den daten in den datenspeicher und dann nach und nach füttern des Netzwerks mit gemischten Patches von verschiedenen patienten. verweis auf fig. 2

4.3 Network Input & Output

4.3.1 Network Input

The input consists of 5 3D volumes (fig. 3) to combine different spatial, anatomical aswell a accelorator information into the training data. the masks are used to achieve a direct connection from accelerator that translates onto the patients anatomy

Beam Shape: beam shape information in form of a volume indicating the trajectory of the beam and its specific shape for each segment. in the masks voxels which the trajecotry passes contain the beam area. this accounts for the outputfactor of the accelerator, meaning that for bigger fields the in-scatter in the central beam line is higher than for smaller fields.

Center Beam Line Distance: The beam of a linear accelerator is best defined in the

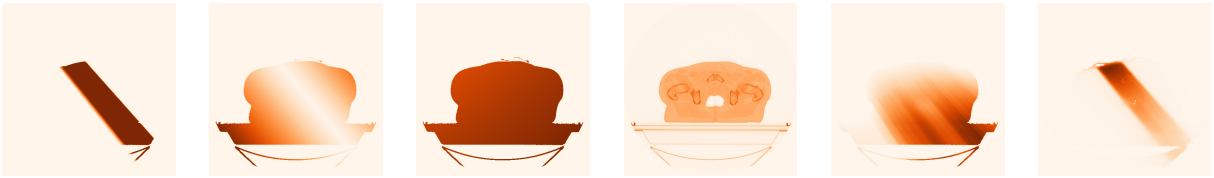

Figure 3: From left to right: Beam Shape Mask, Center Beam Line Distance Mask, Source Distance Mask, CT Mask, Radiological Depth, Target Dose Mask

central beam line. therefore the distance from the central beam line is of importance for the dose deposition. the minimum distance of each voxel from the central beam line accounting voxel dimensionality is saved in this mask.

Source Distance: The square rule of distance for the tissue in which the photons interact and the radiation source is of crucial importance for the dose deposited in the affected tissue. the values in this mask reflect the distance from each voxel to the radiation source with accounting the voxel dimensionality.

CT: Dose deposition and particle interaction in genereal are defined by their energy aswell as the electron density of the affected volume. as the energy of the radiated photons is constant, the impact of the electron density of the volume (in this case the patients anatomy) is accounted in this mask. It consits of the houndsfield units from a ct scan. with this mask dose deposition in denser tissues can be accounted for.

Radiological Depth: as a particle passes trough the affected volume it loses its energy on its path. therefore the depth, which a particle has already passedd inside a tissue is very important for the dose deposition effects that take place. because particles lose their energy faster in dense materials, this affect is accounted for using the radiological depth. it accounts for the distance from the source as well as the electron density of the passed tissue. A depth in a dense material results in a higher radiological depth that the same depth in soft tissue.

To only clip the mask values to the actual patients anatomy, all values in each mask were set to zero where the CT mask had a HU value smaller than 874 (150 values above the HU value for air).

4.3.2 Network Output

The output yielded by the network is the single volume of the predicted dose for the given input. It has the same dimensionality for wudthm height and depth aswell as voxel dimensions as the input masks. shown in fig. 3

4.4 Training Data Generation

The patient anatomy and accelerator information of each segment was extracted from the radio treatment plan. The required masks were created from this information using in-house python scripts. The target dose mask was simulated using the dosxyznrc software tool from the EGSnrc software package (the code is publicly available at https://github.com/nrc-cnrc/EGSnrc). EGSnrc enabled us to us to simulate each beam segment from each patient's treatment plan, with the accurate MR linac accelerator head model frrom previous work at our institution. Each segment was simulated using 10^7 for time efficiency.

hier noch beschreiben wie lange due daten generation braucht? wichtig?

4.5 Evaluation Metrics

to directly asses the quality of the dose prediction, we used the gamma - passrate, which compares two dose distrbutioins on the same grid. in this analysis tool eaach voxel and its value on grid 1 is compared to the zugehörigen voxel from the second dose distribution. two margins are used that define in which margin the seconds dose voxel can vary to be accepted as valid. the two margins are a dose value margin aswell as a spatial margin. hier noch erklären was der spatial margin eigentlich aussagt

heri noch vllt formel und abbildung die auswertungsmetrik

4.6 Hypotheses

These 1: the general dose deposition process for a spcific tumor entity can be learned on data of a multitude of radio treatment plans on that the specific tumor site.

Experiment 1: We therefore train a network on prostate patient treatment plan data and anatomies and assess the quality of predicted dose distribution with the gamma passrate of each segment as well asa the entire plan.

These 2: the in These 1 trained network performes poorly when translating into different tumor sites that were not included in the training data and therefore generalizes poorly.

Experiment 2: To test translational capabilities the network is tested against liver, breast, head & neck and lymph node treatment plan data.

These 3: the includation of different tumor sites into the training data improves the the translational capabilites of the network to other tumor sites, while maintaining high accuracy on the included tumor sites and therefore improve the robustness of the network.

Experiment 3: we therefore train the same network from these 1 on prostate, liver, breast and head & neck treatment plan data. the translational capabilities are then assed by testing with prostate, liver, breast, head & neck and lymph node data. by doing this we asses if the network performance decreases on prostate data by including new tumor sites into the training data and we assess its performance on seen (prostate, liver, heaad & neck, breast) aswell as unseen treatment plan data (lymph nodes).

These 4: The network is capable of learning the underlying physics of the dose depositiopn process.

Experiment 4: By creating phantom input data in the form of a water slap at various positions inside an air volume, we investigate if the network has learned the underlying physics of the dose deposition process.

4.7 Patient Data

All patients gave their informed written consent to this study, which was approved by the local ethical committee (ethics approval No. 659/2017BO1). patient data from our institution previously treated at the mr linac. all plans were created by a medical physicist in agreement with a oncologist Welche Entitäten: Prostate only training: 45 prostate treatment plans with a total of 2342 Segments, 36/4/5 split für train / val / test split. with a mean fieldsize of 36.57 $\pm$ 17.9 cm^2 for training / validation set and 34.57 $\pm$ 15.86 cm^2 for the test set. mixed model 15 prostate with 720 segments , 35.49 $\pm$ 18.01 and 34.57 $\pm$ 15.86 15 liver 819 Segments 24.09 $\pm$ 18.36 and 22.81 $\pm$ 14.47 15 mamma 656 Segments 40.72 $\pm$ 28.48 and 40.60 $\pm$ 37.98 14 head & neck 929 segments in einem 8/2/5 split also in 32/8/20 train / validation / test ratio. aswell as 15 patient plans 659 segments for lymphnodes exclusively for testing with a mean fieldsize of 25.95 $\pm$ 25.59 as you can see in tab. 1 All patients gave their informed written consent to this study, which was approved by the local ethical committee (ethics approval No. 659/2017BO1).

	Prostate-Only	**Mixed-Entity**				**Testing**
		Liver	Mamma	Head & Neck	Prostate	Lymphnodes
Number of Segments	45	15	15	15	15	15
Number of Segments	2342	819	656	929	720	659
Training / Validation / Testing	36/4/5	8/5/2	8/2/5	8/5/2	8/5/2	Only Testing
Fieldsize Training/Validation	36.5 (17.9)	24.1 (18.4)	40.7 (28.5)	63.0 (50.5)	35.5 (18.0)	N/A
Fieldsize Testing	34.5 (15.8)	22.8 (14.4)	40.6 (38.0)	68.9 (53.6)	34.6 (15.9)	26.0 (25.6)

Table 1: Patient data infortmation for Prostate-Only as well as Mixed-Entity trained model and testing data set. Fieldsizes are given as mean (standard deviation).

5 Results

In the following section the experients from each theses to be tested are presented in a chronological manner.

5.1 These 1 / Experiment 1

The training of the network took around 11 days with a batchsize of 128 and $6.7 \cdot 10^5$ patches of size 32x32x32 voxels. The training was performced on 4 nvidia gtx 2080 ti and a initial learning rate of 10^{-4} decreasing by a factor of 10 as soon as the validation loss or the gamma pass rate on the validation set did not decrease for 50 epochs. The training was stopped when no improvement was observed at a learning rate of 10^{-6} for 50 epochs.

The model reaches a mean gamma score of 96.16% ± 6.12% (median: 98.02%) on the test dataset for prostate patients. (fig. 4) shows a qualitative example of a target dose and the respective dose prediction and gamma map for a prostate cancer patient in the isocentric slice.

Figure 4: Dose prediction example on isocentric slice on prostate cancer patient from test cohort with prostate data only trained model. From left to right: target dose; dose prediction; gamma map for isocentric slice with a gamma pass rate of 98.02%

		Liver	**Mamma**	**H&N**	**LK**
Number of Patient Plans	/1	5	5	5	15
Mean Gamma Passrate		77.69	63.25	76.19	82.12
STD Gamma Passrate	/%	10.13	6.72	4.99	11.51
Median Gamma Passrate		80.39	63.48	77.67	85.9

Table 2: Summary of gamma passrates for liver, mamma, head and lyphnodes tumor patients

		Prostate	**Liver**	**Mamma**	**H&N**	**LN**
Number of Patient Plans	/1	5	5	5	5	15
Mean Gamma Passrate		97.85	97.59	87.46	90.68	90.71
STD Gamma Passrate	/%	2.82	4.56	6.61	6.4	9.6
Median Gamma Passrate		98.59	99.92	86.15	92.74	94.19

Table 3: Summary of gamma passrates for liver, mamma, head and lyphnodes tumor patients

5.2 These 2 / Experiment 2

Model performance for liver, mamma and head tumor sites are summarized in (table ...).

5.3 These 3 / Experiment 3

The training of the network took around 9 days with a batchsize of 128 and $5.0 \cdot 10^5$ patches of size 32x32x32 voxels. The training was performced on 4 nvidia gtx 2080 ti and a initial learning rate of 10^{-4} decreasing by a factor 10 as soon as the validation loss or the gamma pass rate on the validation set did not decrease for 50 epochs. The training was stopped when no improvement was observed at a learning rate of 10^{-6} for 50 epochs.

Model performance for prostate, liver, mamma and head tumor sites are summarized in (table ...).

A comparison between prostate only and mixed trained models is depictedd in fig. ....

Single segment analysis gives a deeper insight into the actual performance differences of the model. we therefore assessed the gamma passrate for each single segment of all test data (fig ...). Additional information about performance regarding fieldsize can be benefitial to predict wether an unseen segment will reach high dose conformaty. fig ... shows the analysis for each segment of the test data regarding their fieldsize. additional information about the occurence of each discretized fieldsize range is shown in the background.

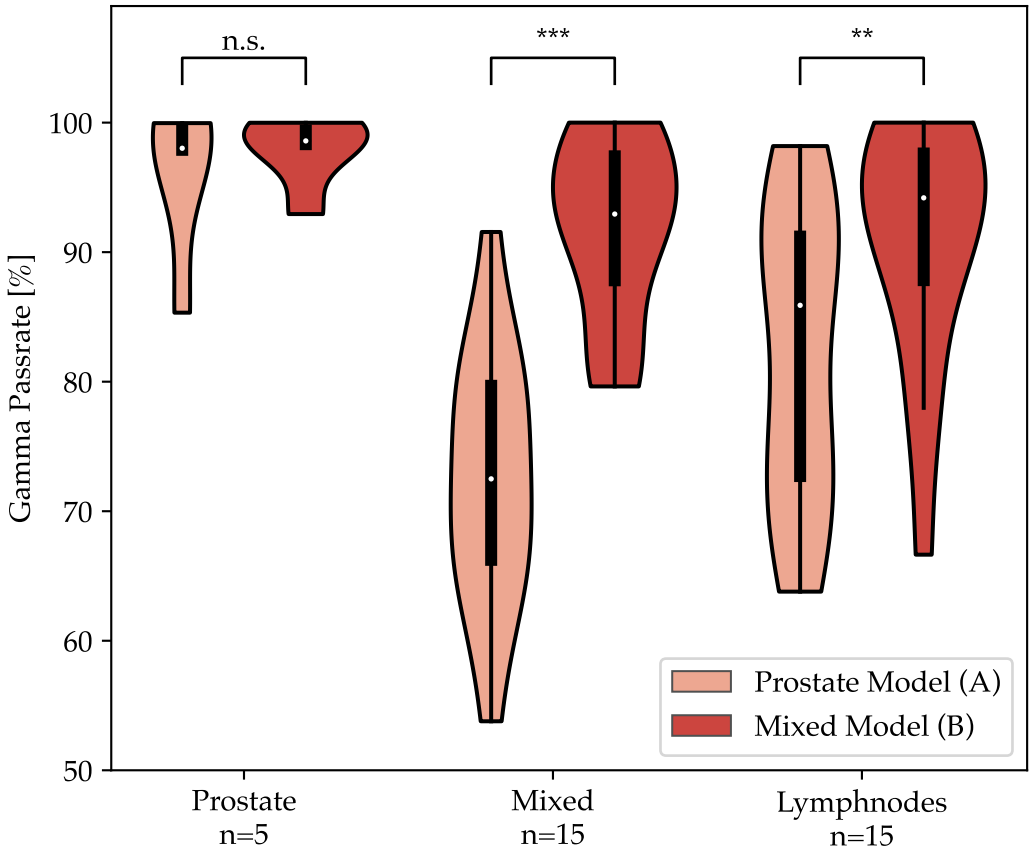

Figure 5: Prediction accuracy comparison between prostate only and mixed trained models. Passrates for liver, mamma and H&N are combined into one group of 'mixed' data. Significance level using a wilcoxon signed-ranked test are shown above the compared dataseries.

5.4 These 4 / Experiment 4

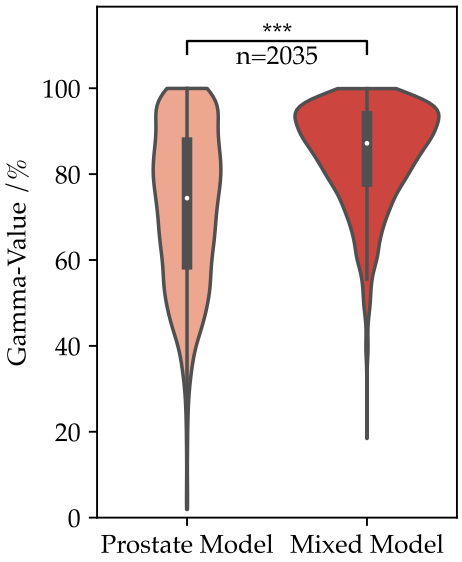

Figure 6: Prediction accuracy for all segments of the test data.

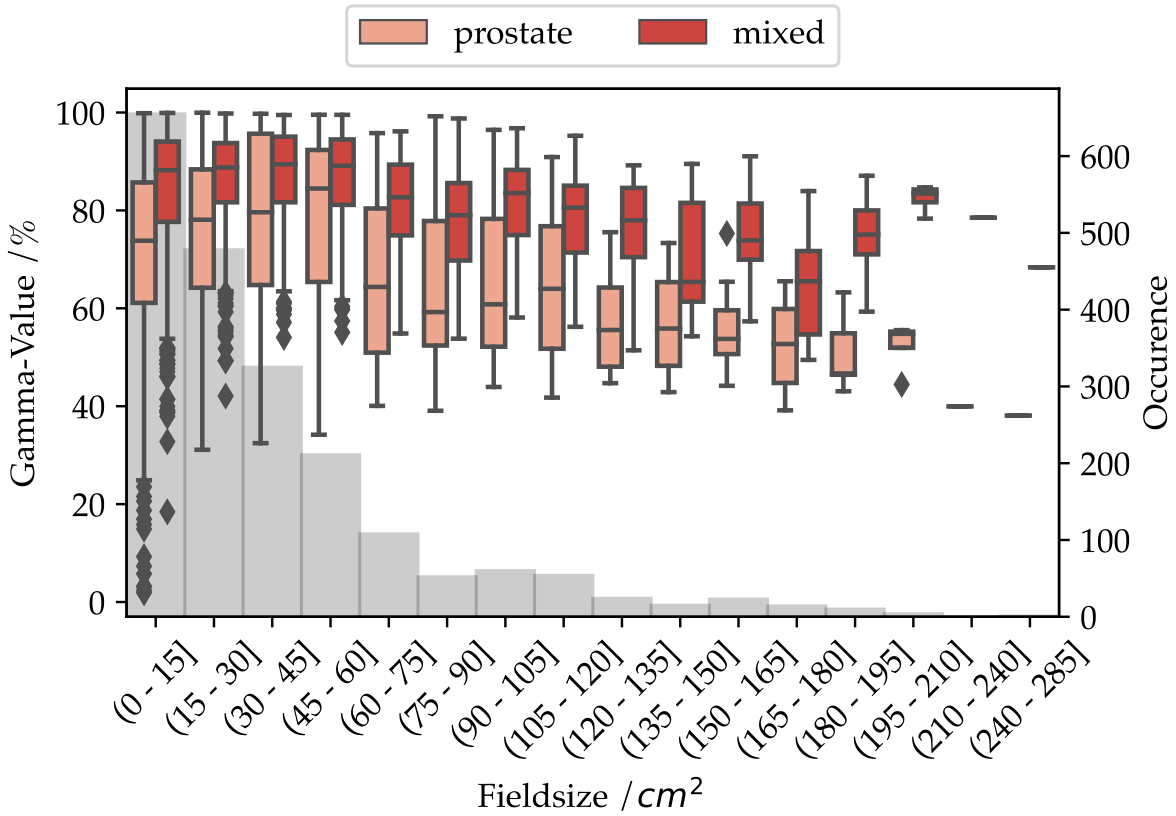

Figure 7: Prediction accuracy of each segment with allocation in terms of field size for prostate only and mixed trained model.

Literature

[1] Hans Geinitz et al.: *3D conformal radiation therapy for prostate cancer in elderly patients*. In: Radiotherapy and Oncology 76.1 (July 2005), 27–34. ISSN: 01678140. DOI: 10.1016/j.radonc.2005.06.001. URL: https://linkinghub.elsevier.com/retrieve/pii/S0167814005002082 (visited on 08/16/2021).

[2] Tan Dat Nguyen et al.: *The curative role of radiotherapy in adenocarcinoma of the prostate in patients under 55 years of age: A rare cancer network retrospective study*. In: Radiotherapy and Oncology 77.3 (Dec. 2005), 286–289. ISSN: 01678140. DOI: 10.1016/j.radonc.2005.10.015. URL: https://linkinghub.elsevier.com/retrieve/pii/S0167814005004779 (visited on 08/16/2021).

[3] Tom Budiharto, Karin Haustermans, and Gyoergy Kovacs: *External Beam Radiotherapy for Prostate Cancer*. In: Journal of Endourology (), 10.

[4] Joseph Ragaz et al.: *Adjuvant Radiotherapy and Chemotherapy in Node-Positive Premenopausal Women with Breast Cancer*. In: The New England Journal of Medicine (1997), 7.

[5] Mario De Lena et al.: *Combined Chemotherapy-Radlotherapy Approach in Locally Advanced (T3b-T4)Breast Cancer*. In: (), 7.

[6] Carolyn Taylor et al.: *Estimating the Risks of Breast Cancer Radiotherapy: Evidence From Modern Radiation Doses to the Lungs and Heart and From Previous Randomized Trials*. In: Journal of Clinical Oncology 35.15 (May 20, 2017), 1641–1649. ISSN: 0732-183X. DOI: 10.1200/JCO.2016.72.0722. URL: https://www.ncbi.nlm.nih.gov/pmc/articles/PMC5548226/ (visited on 08/16/2021).

[7] N. R. Datta et al.: *Head and neck cancers: Results of thermoradiotherapy versus radiotherapy*. In: International Journal of Hyperthermia 6.3 (Jan. 1990), 479–486. ISSN: 0265-6736, 1464-5157. DOI: 10.3109/02656739009140944. URL: http://www.tandfonline.com/doi/full/10.3109/02656739009140944 (visited on 08/16/2021).

[8] S.A. Bhide and C.M. Nutting: *Advances in radiotherapy for head and neck cancer*. In: Oral Oncology 46.6 (June 2010), 439–441. ISSN: 13688375. DOI: 10.1016/j.oraloncology.2010.03.005. URL: https://linkinghub.elsevier.com/retrieve/pii/S1368837510000941 (visited on 08/16/2021).

[9] Pierre Castadot et al.: *Adaptive Radiotherapy of Head and Neck Cancer*. In: Seminars in Radiation Oncology 20.2 (Apr. 2010), 84–93. ISSN: 10534296. DOI: 10.1016/j.semradonc.2009.11.002. URL: https://linkinghub.elsevier.com/retrieve/pii/S1053429609000769 (visited on 08/16/2021).

[10] Howard E. Morgan and David J. Sher: *Adaptive radiotherapy for head and neck cancer*. In: Cancers of the Head & Neck 5.1 (Dec. 2020), 1. ISSN: 2059-7347. DOI: 10.1186/s41199-019-0046-z. URL: https://cancersheadneck.biomedcentral.com/articles/10.1186/s41199-019-0046-z (visited on 08/16/2021).

[11] Morten Høyer et al.: *Radiotherapy for Liver Metastases: A Review of Evidence*. In: International Journal of Radiation Oncology*Biology*Physics 82.3 (Mar. 1, 2012), 1047–1057. ISSN: 0360-3016. DOI: 10.1016/j.ijrobp.2011.07.020. URL: https://www.sciencedirect.com/science/article/pii/S0360301611030902 (visited on 08/16/2021).

[12] Jörn Wulf et al.: *Stereotactic Radiotherapy of Targets in the Lung and Liver:* in: Strahlentherapie und Onkologie 177.12 (Dec. 2001), 645–655. ISSN: 0179-7158. DOI: 10.1007/PL00002379. URL: http://link.springer.com/10.1007/PL00002379 (visited on 08/16/2021).

[13] Joern Wulf et al.: *Stereotactic radiotherapy of primary liver cancer and hepatic metastases*. In: Acta Oncologica 45.7 (Jan. 2006), 838–847. ISSN: 0284-186X, 1651-226X. DOI: 10.1080/02841860600904821. URL: http://www.tandfonline.com/doi/full/10.1080/02841860600904821 (visited on 08/16/2021).

[14] Florian Sterzing et al.: *Stereotactic body radiotherapy for liver tumors: Principles and practical guidelines of the DEGRO Working Group on Stereotactic Radiotherapy*. In: Strahlentherapie und Onkologie 190.10 (Oct. 2014), 872–881. ISSN: 0179-7158, 1439-099X. DOI: 10.1007/s00066-014-0714-1. URL: http://link.springer.com/10.1007/s00066-014-0714-1 (visited on 08/16/2021).

[15] Jacob S Witt, Stephen A Rosenberg, and Michael F Bassetti: *MRI-guided adaptive radiotherapy for liver tumours: visualising the future*. In: The Lancet Oncology 21.2 (Feb. 1, 2020), e74–e82. ISSN: 1470-2045. DOI: 10.1016/S1470-2045(20)30034-6. URL: https://www.sciencedirect.com/science/article/pii/S1470204520300346 (visited on 08/16/2021).

[16] Breast Cancer Expert Panel of the German Society of Radiation Oncology (DEGRO) et al.: *DEGRO practical guidelines for radiotherapy of breast cancer IV: Radiotherapy following mastectomy for invasive breast cancer*. In: Strahlentherapie und Onkologie 190.8 (Aug. 2014), 705–714. ISSN: 0179-7158, 1439-099X. DOI:

10.1007/s00066-014-0687-0. URL: http://link.springer.com/10.1007/s00066-014-0687-0 (visited on 08/16/2021).

[17] Haruo Matsushita et al.: *Stereotactic Radiotherapy for Oligometastases in Lymph Nodes—A Review*. In: Technology in Cancer Research & Treatment 17 (Jan. 2018), 153303381880359. ISSN: 1533-0346, 1533-0338. DOI: 10.1177/1533033818803597. URL: http://journals.sagepub.com/doi/10.1177/1533033818803597 (visited on 08/16/2021).

[18] John L. Mikell et al.: *Postoperative Radiotherapy is Associated with Better Survival in Non–Small Cell Lung Cancer with Involved N2 Lymph Nodes: Results of an Analysis of the National Cancer Data Base*. In: Journal of Thoracic Oncology 10.3 (Mar. 2015), 462–471. ISSN: 15560864. DOI: 10.1097/JTO.0000000000000411. URL: https://linkinghub.elsevier.com/retrieve/pii/S1556086415316543 (visited on 08/16/2021).

[19] Dan Lundstedt et al.: *Long-term symptoms after radiotherapy of supraclavicular lymph nodes in breast cancer patients*. In: Radiotherapy and Oncology 103.2 (May 2012), 155–160. ISSN: 01678140. DOI: 10.1016/j.radonc.2011.12.017. URL: https://linkinghub.elsevier.com/retrieve/pii/S0167814011007572 (visited on 08/16/2021).

[20] Barbara Alicja Jereczek-Fossa, Sara Ronchi, and Roberto Orecchia: *Is Stereotactic Body Radiotherapy (SBRT) in lymph node oligometastatic patients feasible and effective?* In: Reports of Practical Oncology and Radiotherapy 20.6 (2015), 472–483. ISSN: 1507-1367. DOI: 10.1016/j.rpor.2014.10.004. URL: https://www.ncbi.nlm.nih.gov/pmc/articles/PMC4661354/ (visited on 08/16/2021).

[21] Samaneh Kazemifar et al.: *Segmentation of the prostate and organs at risk in male pelvic CT images using deep learning*. In: Biomedical Physics & Engineering Express 4.5 (July 23, 2018), 055003. ISSN: 2057-1976. DOI: 10.1088/2057-1976/aad100. URL: https://iopscience.iop.org/article/10.1088/2057-1976/aad100 (visited on 08/23/2021).

[22] Shujun Liang et al.: *Deep-learning-based detection and segmentation of organs at risk in nasopharyngeal carcinoma computed tomographic images for radiotherapy planning*. In: European Radiology 29.4 (Apr. 2019), 1961–1967. ISSN: 0938-7994, 1432-1084. DOI: 10.1007/s00330-018-5748-9. URL: http://link.springer.com/10.1007/s00330-018-5748-9 (visited on 08/23/2021).

[23] Dinggang Shen et al., eds.: *Medical Image Computing and Computer Assisted Intervention – MICCAI 2019: 22nd International Conference, Shenzhen, China, October 13–17, 2019, Proceedings, Part II*. Vol. 11765. Lecture Notes in Computer Science. Cham: Springer International Publishing, 2019. ISBN: 978-3-030-32244-1 978-3-030-32245-8. DOI: 10.1007/978-3-030-32245-8. URL: https://link.springer.com/10.1007/978-3-030-32245-8 (visited on 08/23/2021).

[24] Jiawei Fan et al.: *Automatic treatment planning based on three-dimensional dose distribution predicted from deep learning technique*. In: Medical Physics 46.1 (Jan. 2019), 370–381. ISSN: 00942405. DOI: 10.1002/mp.13271. URL: http://doi.wiley.com/10.1002/mp.13271 (visited on 03/16/2021).

[25] Zhiqiang Liu et al.: *A deep learning method for prediction of three-dimensional dose distribution of helical tomotherapy*. In: Medical Physics 46.5 (May 2019), 1972–1983. ISSN: 0094-2405, 2473-4209. DOI: 10.1002/mp.13490. URL: https://onlinelibrary.wiley.com/doi/abs/10.1002/mp.13490 (visited on 03/16/2021).

[26] C. Kontaxis et al.: *DeepDose: Towards a fast dose calculation engine for radiation therapy using deep learning*. In: Physics in Medicine & Biology 65.7 (Apr. 2020). Publisher: IOP Publishing, 075013. ISSN: 0031-9155. DOI: 10.1088/1361-6560/ab7630. URL: https://doi.org/10.1088/1361-6560/ab7630 (visited on 08/23/2021).

[27] Ti Bai et al.: *Deep dose plugin: towards real-time Monte Carlo dose calculation through a deep learning-based denoising algorithm*. In: Machine Learning: Science and Technology 2.2 (June 1, 2021), 025033. ISSN: 2632-2153. DOI: 10.1088/2632-2153/abdbfe. URL: https://iopscience.iop.org/article/10.1088/2632-2153/abdbfe (visited on 08/23/2021).

[28] Xiao Han: *MR-based synthetic CT generation using a deep convolutional neural network method*. In: Medical Physics 44.4 (2017). _eprint: https://aapm.onlinelibrary.wiley.com/do 1408–1419. ISSN: 2473-4209. DOI: 10.1002/mp.12155. URL: https://aapm.onlinelibrary.wiley.com/doi/abs/10.1002/mp.12155 (visited on 08/23/2021).

[29] Jelmer M. Wolterink et al.: *Deep MR to CT Synthesis Using Unpaired Data*. In: *Simulation and Synthesis in Medical Imaging*. Ed. by Sotirios A. Tsaftaris et al. Lecture Notes in Computer Science. Cham: Springer International Publishing, 2017, 14–23. ISBN: 978-3-319-68127-6. DOI: 10.1007/978-3-319-68127-6_2.

[30] Anna M. Dinkla et al.: *MR-Only Brain Radiation Therapy: Dosimetric Evaluation of Synthetic CTs Generated by a Dilated Convolutional Neural Network*. In: International Journal of Radiation Oncology*Biology*Physics 102.4 (Nov. 2018),

801–812. ISSN: 03603016. DOI: 10.1016/j.ijrobp.2018.05.058. URL: https://linkinghub.elsevier.com/retrieve/pii/S0360301618309106 (visited on 08/23/2021).

Apendix